1 **An overview on the airborne measurement in Nepal,-part 1: vertical profile of aerosol size-number,**

2 **spectral absorption, and meteorology**

3

4 Ashish Singh[1]*, Khadak S. Mahata[1], Maheswar Ruphaketi[1]*, Wolfgang Junkermann[2], Arnico K. Panday[3],

5 Mark G. Lawrence[1]

6 [1]Institute for Advanced Sustainability Studies, Potsdam, Germany

7 [2]Institute of Meteorology and Climate Research, IMK-IFU, Garmisch-Partenkirchen, Germany

8 [3]International Centre for Integrated Mountain Development (ICIMOD), Lalitpur, Nepal

9

10 *Corresponding author: Ashish Singh (ashish.singh@iass-potsdam.de) and

11 Maheswar Rupakheti (maheswar.rupakheti@iass-potsdam.de)

12

13   **Abstract**

14        The paper provides an overview of an airborne measurement campaign with a microlight aircraft,

15   over the Pokhara Valley region, Nepal, a metropolitan region in the central Himalayan foothills. This is

16   the first aerial measurements in the central Himalayan foothill region, one of the polluted but relatively

17   poorly sampled regions of the world. Conducted in two phases (in May 2016 and December 2016-

18   January 2017), the goal of the overall campaign was to quantify the vertical distribution of aerosols over

19   a polluted mountain valley in the Himalayan foothills, as well as to investigate the extent of regional

20   transport of emissions into the Himalayas. This paper summarizes results from first phase where test

21   flights were conducted in May 2016 (pre-monsoon), with the objective of demonstrating the potential of

22   airborne measurements in the region using a portable instrument package (size with housing case: 0.45

23   m x 0.25 m x 0.25 m, 15 kgs) onboard an ultralight aircraft (IKARUS-C42). A total of five sampling test

24   flights were conducted (each lasting for 1-1.5 h) in the Pokhara Valley to characterize vertical profiles of

25   aerosol properties such as aerosol number and size distribution (0.3-2 µm), total particle concentration

26   (>14 nm), aerosol absorption (370-950 nm), black carbon (BC), and meteorological variables. Although

27   some interesting observations were made during the test flight, the study is limited to a few days (and

28   only a few hours of flight in total) and thus, the analysis presented may not represent the entire

29   pollution-meteorology interaction found in the Pokhara Valley

30        The vertical profiles of aerosol species showed decreasing concentrations with altitude (815 to

31   4500 m a.s.l.); steep concentration gradient below 2000 m (a.s.l.) in the morning and mixed profiles (up

32   to ca. 4000 m a.s.l.) in the afternoon. The near-surface (<1000 m a.s.l.) BC concentrations observed in

33   the Pokhara Valley were much lower than pre-monsoon BC concentrations in the Kathmandu Valley,

34   and similar in range to Indo-Gangetic Plain (IGP) sites such as Kanpur in India.  The sampling test flight

35   also detected an elevated polluted aerosol layer (around 3000 m a.s.l.) over the Pokhara Valley, which

36   could be associated with the regional transport. The total aerosol and black carbon concentration in the

37   polluted layer was comparable with the near-surface values (<1000 m a.s.l.). The elevated polluted layer

38   was also characterized by high aerosol extinction coefficient (at 550 nm) and was identified as smoke

39   and a polluted dust layer. The observed shift in the westerlies (at 20-30° N) entering Nepal during the

40   test flight period could be an important factor for the presence of elevated polluted layers in the

41   Pokhara Valley.

42

## 1. Introduction

The Himalayas and surrounding regions are one of the unique ecosystems in the world, with a great variety in the geography and socio-economics, and a notable significance in the context of regional and global environmental change.  Areas in the foothills of the Himalayas still constitute large regions of rural populations along with pockets of rapidly growing cities. Consequently, there is a complex interaction among changing emission sources and their interaction with regional and global climate change. Among emitted air pollutants, the chemical and physical properties of aerosols have been linked to significant burdens of disease, to melting of glaciers, to crop loses, to hydrological changes and to cloud properties (Bollasina et al., 2011;Vinoj et al., 2014;Lau, 2014;Burney and Ramanathan, 2014;Brauer et al., 2012;Cong et al., 2015;Li et al., 2016).

Sources of aerosols in the Himalayas and the nearby Indo-Gangetic Plain (IGP) typically vary between urban, peri-urban and rural locations; fossil fuel and industrial emissions such as vehicles, brick kilns, waste burning, cement factories etc., are typically urban and peri-urban; biomass cookstove, agriculture and waste burning and forest fires are often linked to emissions from rural areas (Guttikunda et al., 2014;Venkataraman et al., 2006;Stone et al., 2010). Secondary chemical pathways also contribute to the aerosols in the ultrafine and accumulation-mode range via particle formation events (Venzac et al., 2008;Neitola et al., 2011).

Aerosol properties in the Himalayas have large spatial and temporal variations, especially in the pre-monsoon and monsoon season. These observed variations are influenced by emission sources, regional meteorology, and geography (Dey and Di Girolamo, 2010). The influence of aerosol particles on local and regional weather during these adjacent seasons has significant implications for timing, intensity and spatial distribution of the summer monsoon in the region (Bollasina et al., 2011;Ramanathan et al., 2001). Studies describing the aerosol-meteorology interaction are often missing in the Himalayan region partly due to lack of surface and airborne measurements of aerosol properties along with meteorology. Most past campaign-mode measurements in the Himalayan regions, to our knowledge, have been ground measurements, which have aided in evaluating aerosol properties, and their transformation and transport mechanisms (Shrestha et al., 2013;Shrestha et al., 2010;Ramana et al., 2004;Marcq et al., 2010;Panday and Prinn, 2009;Cho et al., 2017). Long-term continuous measurements of aerosols and meteorology are limited to a few stations in the High Himalayas, such as the recently discontinued Nepal Climate Observatory at Pyramid (NCO-P, 27.95° N, 86.81° E, 5050 m a.s.l.), a high altitude observatory located near basecamp of Mt. Everest. Columnar and satellite measurements such as AERONET and CALIPSO have provided a regional overview of aerosol type and vertical distribution, as well as

3

75  estimation of the aerosol heating rate in the atmospheric column (Kuhlmann and Quaas, 2010;Gautam

76  et al., 2011;Pandey et al., 2017). However, these measurement techniques often suffer from large

77  uncertainty and biases while retrieving the complex nature of the aerosols observed in the region (Jai

78  Devi et al., 2011).

79      Regional meteorology in the 850-500 mb range plays an important role in the transformation and

80  transport of aerosols from Western Asia to the IGP, the Himalayan foothills, the Himalayan and Tibetan

81  Plateau region (Decesari et al., 2010;Marinoni et al., 2013;Lüthi et al., 2015). At these altitudes,

82  synoptic- scale air masses are mostly westerly/northwesterly during the pre-monsoon and

83  southwesterly/easterly during the monsoon. These air masses are often linked to dust aerosol transport

84  during the pre-monsoon season from Western Asia into the Himalayas, including populated mountain

85  valley such as Kathmandu and Pokhara Valley in Nepal. The transported dust aerosol also mixes with the

86  primary emission (or anthropogenic aerosols) in the IGP and accumulates from northern to eastern IGP

87  along the Himalayan foothills (Gautam et al., 2009b;Gautam et al., 2011). The total aerosol loading is

88  often the highest during the pre-monsoon season in the IGP (Gautam et al., 2009a;Raatikainen et al.,

89  2014), intensified further by weak surface/zonal winds and numerous open biomass burning and forest

90  fires events (Kaskaoutis et al., 2012). The polluted aerosol layer in the IGP is advected into the Himalayas

91  by synoptic-scale westerlies (~500 mb) and also by the valley wind circulation within or along the

92  planetary boundary layer (PBL) (Lüthi et al., 2015). The advection is also facilitated by the strong updraft

93  and PBL expansion (the highest in the pre-monsoon in the IGP) often mixing with the synoptic-scale

94  westerlies (Raatikainen et al., 2014).  Because of strong convective activity in the IGP, the polluted air

95  masses near the surface are often lifted up to 5-7 km or higher (Kuhlmann and Quaas, 2010). In addition

96  to the synoptic-scale transport, thermally-driven valley winds also enable the transport of humid and

97  polluted air mass (with enhanced absorbing fraction) from IGP into the Himalayan foothills, and further

98  up into the mountain valleys and elevated locations (Raatikainen et al., 2014;Lüthi et al., 2015;Gogoi et

99  al., 2014;Putero et al., 2014;Decesari et al., 2010;Marcq et al., 2010). Strongly coupled with the

100 expansion of the PBL in the IGP, the upslope movement of polluted air masses into the foothills and

101 further east is characterized by late afternoon peaks in aerosol optical depth (AOD) in many

102 measurement sites along the Himalayan range such as Hanle Valley (Ladakh, India), Mukteswar and

103 Manora site (Nainital, India), Hetauda (Nepal), Langtang Valley (Nepal), Dhulikhel (Nepal), Kathmandu

104 Valley (Nepal) and NCO-P (Nepal). The temporal and spatial extent of this observed "ventilation" at

105 multiple locations could be indicative of a regional-scale transport than mesoscale (Gogoi et al.,

106 2014;Raatikainen et al., 2014;Gautam et al., 2011;Putero et al., 2015;Marcq et al., 2010).

107      To date, there have been no observations of vertical distributions of aerosol and gaseous species

108    carried out in the Himalayan region. Therefore, the airborne measurement campaign was designed to

109    address two major questions: (i) what is the variation in the aerosol properties, notably the vertical

110    distributions, over a polluted mountain valley, and (ii) what is the quantitative extent of regional

111    transport of aerosols in the higher Himalayas? The campaign was carried out in two phases in the

112    Pokhara Valley and surrounding areas in Nepal.  In the first phase, test flights were conducted in May

113    2016 and in the second phase, intensive sampling flights were carried out in December 2016-January

114    2017. This paper provides an overview of the measurement campaign and results from the test flights in

115    May 2016 which include snapshots of vertical profiles of aerosol size, number, and composition, along

116    with meteorological parameters. The airborne measurements presented in this paper are supplemented

117    with observations of local and regional meteorology, as well as satellite and ground-based column-

118    integrated aerosol microphysics and radiative properties (see section 3.1.1 and 3.1.2, also

119    Supplementary S7). A companion paper will follow with more detailed observations and results based

120    on the intensive measurements carried out during December 2016-January 2017.

121

122    **2.   Ultralight measurements in Nepal**

123    *2.1.  Details of the airborne measurement unit*

124       A single-engine two-seater microlight aircraft (IKARUS C-42, COMCO IKARUS, Germany) was used as

125    the aerial platform. The technical specification of the aircraft includes approximately 4 h of flying time, a

126    short take-off run, an additional payload of up to 50 kg, and it is suitable for small spiral movement in

127    the air.  The aircraft has a cruising speed of 165 $kmh^{-1}$, and a 5-6 $ms^{-1}$ rate of climb which makes it an

128    appropriate aerial vehicle to perform measurements at altitudes within the PBL and as close as 50 m

129    above ground level. More detail about the aircraft is available here (http://www.comco-

130    ikarus.de/Pages/c42a-technik.php?lang=en). Its size, speed, and maneuverability offered a decent climb

131    to the free troposphere to capture vertical profiles in the rough terrains of Nepal. The aircraft used for

132    the study is operated by the Pokhara Ultralight Company for recreational flights around the Pokhara

133    Valley.

134       The instrument package was specifically designed and tested for aerial measurements (Junkermann,

135    2001). Table 1 describes each instrument and the integration performed to prepare the package for the

136    aerial deployment.  The instrument package consists of a GRIMM OPS (optical particle spectrometer)

137    model 1.108 for particle size distributions (0.3 to 20 µm, 16 size bins)  with sampling frequency of 6 s,

138  and a TSI condensation particle counter (CPC) 3760 for total particle concentration (>14 nm) at 1 s

139  resolution (See Figure S1 in the supplement). The package also included a Magee Scientific aethalometer

140  (AE42) for aerosol absorption at seven different wavelengths (370 -950 nm).  The instruments were

141  reduced in weight for use on the aircraft. The CPC was operated with a constant mass flow and an

142  internal direct current (DC) pump instead of the original flow regulation by a critical orifice.

143  Meteorological parameters including temperature and dew point were sampled at a rate of 1 s using

144  METEOLABOR (TPS3). All the sensors were connected to a modular computer (PC104) for data

145  acquisition. The PC104 is also equipped with a Global Positioning System (GPS), and multiple serial and

146  analog connectors. For inflight instrument checks and quick online overview of the atmospheric

147  conditions, a small liquid crystal display (LCD) was also connected to the PC104 and placed in the cockpit

148  areas for the flight crew. This display showed real-time aerosol number concentrations and

149  meteorological parameters.

150  **Table 1. Instrument package deployed in the microlight aircraft**

151      The instrument package weighs approximately 15 kg and consumes <60 W, well within the

152  power supply range of the aircraft battery. It is housed in an aluminum box (0.45 m x0.25 mx0.25 m) and

153  can be easily integrated with a mobile platform such as the IKARUS (See Figure S1). In IKARUS, the

154  instrument was placed in the rear section behind the seats which is otherwise almost empty or used for

155  cargo, and only contains the fuel tank and supporting aluminum bars. The sample inlet line (internal

156  diameter of 0.004 m or ~4.0 mm ID brass tubing) ran along the wingspan and was approximately 1.8 m

157  (in length, sampling tube) from the cockpit. Once the sample line is inside the aircraft, it is distributed to

158  all the aerosol instruments using a simple metal flow splitter (0.006 m ID). No external pump was used

159  to pull the aerosol into the sampling line, the total flow (~ 3.0 lpm) in the sampling line (before the split)

160  was due to the internal pump of all the instruments. The sample inlet positioning at the end of the

161  wingspan also minimizes the influence of the aircraft propeller, located in the front of the cockpit.

162  *2.2.   Site description*

163      Pokhara Valley is Nepal's second largest populated valley (pop. >250,000) after the Kathmandu

164  Valley (CBS, 2011).  The valley is approximately at 815 m (a.s.l.), ~150 km west of the Kathmandu Valley,

165  and ~90 km northeast of the southern plains (~100 m a.s.l.) bordering IGP. The valley is surrounded by

166  mountains which are approximately 1000-2000 m (a.s.l.). Further north of the Pokhara Valley, within 30

167  km the elevation gradient increases rapidly to over 7000 m (a.s.l.) or higher (see Figure 1). This steep

168   elevation gradient is conducive for the orographic lift of humid air masses, and thus the valley also

169   receives one of the highest rates of precipitation in Nepal and occasional strong convective updrafts

170   leading to hailstorms and thunderstorms (Aryal et al., 2015). The mixing of dry westerly air masses with

171   heated moist air masses from the Bay of Bengal produces strong convection over the Pokhara Valley,

172   and thus results in strong updrafts. These strong convective activities are frequent in the pre-monsoon

173   and monsoon season but do not occur during the winter season.

174   *2.3. Test flight patterns over the Pokhara Valley*

175       Five test flights were conducted in the morning and evening period around Pokhara Valley (83.97°

176   E, 28.19° N, 815 m a.s.l.) with each flight lasting for about 1 to 1.5 h from 5-7 May 2016. The flight

177   pattern was consistently flown over the northwest part of the valley (Figure 1).  A typical flight

178   commenced from the Pokhara Regional Airport (818 m a.s.l.) and steadily flew 5-10 km northwest along

179   the Pokhara Valley leaving the direct airport vicinity toward the Himalayas. This was followed by spirals

180   up and down sampling from approximately 1000 to 4000 m, often reaching close to the lower base of

181   the clouds in the free troposphere. Further climbs into the cloud layer were avoided during the test

182   flights.

183   **Figure 1.**  A typical test flight within the Pokhara Valley on 5 May 2016.  The plot is generated using a
184   Matlab-Google Earth toolbox (https://www.mathworks.com/matlabcentral/fileexchange/12954-google-
185   earth-toolbox). Each dot is a single sample point (sampling frequency of 1Hz); the color of the dot
186   indicates the total aerosol number concentration and the value of each color is shown as a color bar.

187   *2.4. Data processing and quality*

188       The data from all the instruments was synced with the GPS clock, and the PC104 received all the

189   data simultaneously and creates a common time-stamped data file. Prior to each test flight, a zero test

190   was conducted to identify any possible leaks in the sample line.

191       The collected data from the five test flights went through multiple steps of quality control and

192   quality assurance. Occasionally during the radio communication by the pilot with the ground station or

193   air traffic controller, the CPC and the temperature sensor would record exceedingly high values.  This

194   noise is an interference picked up by the sensors from the 5 W radio transmission. The CPC and

195   aethalometer is also sensitive to vibration in the aircraft, especially during upward and downward spiral

196   motion, which may result in flow imbalance in these analyzers. This resulted in random noise segments

197   for a few seconds in the data, which were flagged and not included in the analysis.

198    **3.   Results**

199    *3.1.  General meteorology and air quality, aerosol properties in the Pokhara Valley*

200

201    3.1.1.   *Local and synoptic meteorology in the Pokhara Valley*

202    Climatologically, Pokhara Valley has a humid subtropical climate, characterized by a summer

203    monsoon season from late June to September, preceded by a dry pre-monsoon (March-May, see Figure

204    S2 in the supplement). Dominant winds in the valley are from the southeast and southwest with a strong

205    diurnal variability in the wind speed (Aryal et al., 2015). On a local/regional, the winds in May 2016 were

206    predominantly from the southeast with only occasional strong winds from the southwest (see Figure S3

207    in the supplement, using data available at the regional meteorological station at the Pokhara Airport).

208    During the test flight period (5-7 May 2016), the wind was similar in directionality, with an hourly mean

209    wind speed of 1.8 to 3.0 ms$^{-1}$, with low wind speed (<2.0 ms$^{-1}$) before noon, usually from the southeast,

210    followed by stronger winds from the southwest and northwest (>2.4 ms$^{-1}$) which can continue until late

211    night. The increased wind speed in the afternoon could be katabatic in nature as a result of differential

212    heating of the mountain valley slopes and could be linked to pollution transport from surrounding

213    regions (Gautam et al., 2011).

214    Three dominant synoptic meteorology regimes characterize the seasonality of South Asia

215    (Lawrence and Lelieveld, 2010). They are summer (June-September), the winter monsoon (mid-

216    November to February) and the monsoon-transition periods, which include the pre-monsoon season

217    (March-May) and post-monsoon season (mid-September to mid-November). These synoptic regimes are

218    also active in the Himalayas, including the Pokhara Valley.  The monsoon transition period, during which

219    the test flights were conducted, is characterized by westerlies over 20-30° N at 850 mb and above (see

220    Figure 2). Figure 2 shows the daily wind vector over South Asia for 3, 5, 6 and 7 May 2016 generated

221    using the NCEP NCAR Reanalysis data at 2.5°x 2.5° horizontal resolution. While the reanalysis data can

222    be expected to represent the synoptic-scale phenomena in this region reasonably well, the rough terrain

223    in the Himalayas presents a significant challenge for modeling and the data is thus likely to suffer from

224    biases and other deviations from the observed meteorology (Xie et al., 2007). The wind vector at 850

225    mb in the 20-30° N latitude band was westerly with variable wind speeds in the IGP region near the

226    Himalayan foothills. The wind direction varies diurnally at the 850 mb level, with the wind direction

227    shifting to southwesterly near the Himalayan foothills.  Westerlies were also generally prevalent at the

228    500 mb; however, in the mid-latitudes between 40-50° N (Central Asia) , a trough and crest-like feature

229    of the westerlies moving from west to east Asia is visible (also observed by Lüthi et al., 2015), which was

230    also present prior to the study period. This wind feature was colder and more humid (see Figure S4 in

231    the supplementary material) than the westerlies observed between 20-30° N.  The meandering features

232    (i.e., trough and crest) observed between 40-50° N affects the direction and magnitude of air masses (at

233    20-30° N) entering Nepal. For instance, the crest feature of the westerly was prevalent over the IGP and

234    Nepal prior to 3 May, transitions into the trough feature after the 3$^{rd}$ and continues during the study

235    period. The prevalence of the trough was characterized by the intrusion of wind into lower latitudes as

236    well as into the IGP, also indicated by the change in the temperature and humidity (Figure S4). The

237    intrusions of mid-latitude air masses also influence the westerlies entering Nepal in the 20-30° N sector

238    (Lüthi et al., 2015).  As discussed later, variations in the vertical profiles of aerosols above 3000 m (a.s.l.)

239    could be associated with variations observed in these upper layer winds.

240

241    **Figure 2.**  Daily wind vector data at 850 and 500 mb, plotted using the NCEP NCAR reanalysis (2.5° x 2.5°)

242    data over South Asia from 1-7 May 2016. The colors indicate the wind speed in ms$^{-1}$. The plots were

243    generated using the default setup at www.esrl.noaa.gov/psd/data/composites/day/.

244

245  3.1.2.    Overview of the aerosol properties in the Pokhara Valley during the test flight period

246         The variation in aerosol loading (as reflected by AOD) reveals a strong seasonality in the Pokhara

247    Valley (see supplementary figure S7 for a detailed description of aerosol properties in the Pokhara Valley

248    during 2010-2016). The pre-monsoon season (also the time of the test flight) has the highest AOD values

249    (AOD$_{500nm}$>0.6: Figure S7, S7a, S7a, and S5) followed by the monsoon low (AOD$_{500nm}$ ~0.2-0.3), most likely

250    due to the wet removal of aerosols. AOD gradually increased (to ~0.4-0.5) during the post-monsoon

251    through winter to the pre-monsoon season. Generally, the increase of total AOD (sum of fine and

252    coarse) over the Pokhara Valley is dominated by fine-mode aerosol particles, except during the pre-

253    monsoon and monsoon season, when a substantial fraction of coarse-mode particles were also present.

254    The dominant aerosol in the Pokhara Valley is mostly *BC–like* (Giles et al., 2012), based on the values of

255    absorption and extinction Ångstrom exponent (AAE and EAE at 440-870 nm); however, a substantial

256    seasonal variation was observed from more mixed or dust-like in the pre-monsoon months, to more BC-

257    like in the post-monsoon and winter months.

258    **Figure 3.** AOD and other data products from the Level1.5 AERONET direct product in the Pokhara Valley

259    from 1-10 May 2016. The top panel includes AOD at 500nm and the AOD for coarse and fine modes (as

260    shown in figure above as AOD-C, AOD-F). The bottom panel includes the Ångström Exponent (AE) for

261  440-870nm, the fine mode fraction and the visibility (km). The visibility data was available from the
262  synoptic meteorology data available at http://www7.ncdc.noaa.gov/CDO/cdo

263      The aerosol optical properties (columnar) and synoptic meteorology are shown in Figure 3 and
264  Figure S6 (in the supplementary). Prior to the flights days (1-4 May), higher AOD values were recorded in
265  the Pokhara Valley (AOD>1) and dominated by a fine-mode fraction (~0.95). Hazy condition and low
266  visibility (≤5 km) was recorded during the period in the valley (see Figure S6).  Moving into the flight
267  days, the AOD values decreased below 1, markedly by the drop in the fine-mode fraction and the
268  improvement in haze condition and visibility. The flight day periods were also characterized by the
269  presence of scattered clouds and thunderstorms (with no precipitation) in the afternoon, which also
270  imply conditions for the strong vertical mixing of pollutants. It is indicative from Figure 3 and Figure S7
271  that the presence of high levels of pollution over the region from 1-4 May is followed by a short period
272  of (relatively) cleaner conditions, which also coincides with the changes in the synoptic situation
273  observed in the winds at 500 mb (described in section 3.1.1.)

274

275  3.2.    Vertical profiles of absorbing aerosols, particle number and size distribution, temperature, and
276        dew point

277

278      The five test flights are labeled as F1-5 in Figure 4, except F3 which is shown in the supplement (Fig.
279  S10). F1 and F2 were conducted on 5 May, F3 and F4 on 6 May and F5 on 7 May 2016. Due to limitations
280  of the flight permit, the test flights were conducted remaining within the Pokhara Valley as indicated by
281  Figure 1. Among the five sampling flights, F1, F3, and F5 were morning flights, and F2 and F4 were
282  afternoon flights (for details on sampling flights, see Table T1 in the supplement).

283  **Figure 4.** Vertical profiles of aerosol species and meteorological parameters during the 5-7 May 2016
284  test flights in the Pokhara Valley using the IKARUS microlight aircraft. The subplot in each row is
285  arranged by (**i**) size distribution measured by the GRIMM OPS 1.108 (0.3-20 μm), limited to 1 μm in the
286  figure, (**ii**) Total particle number concentration (also indicated as *TPC*,  Dp >14 nm) measured by the CPC
287  3760, along with absorbing aerosol mass density at 370 nm and 880 nm (**iii**) temperature (red line, in °C)
288  and dew point (black dots, in °C) and relative humidity (or RH %), (**iv**) calculated absorption Ångstrom
289  exponent averaged for every 500 meters elevation band. For the size distribution plot, the x-axis
290  represents the optical diameter of the aerosol (nm), and the color bar represents the concentration ($10^x$
291  in #cm$^{-3}$). Of the five test flights, only F1-2, F4-5 is shown here, F3 is in the supplementary. Number size
292  distribution data from Flight F3 is not available due to the failure of the Grimm's pump during flight

293  initiation. In each subplot, the y-axis is the altitude above the mean sea level (in m).  The origin of the y-
294  axis is at 815 m (a.s.l.).

295  3.2.1.  Diurnal variation in the vertical profiles

296      All the vertical aerosol profiles (Figure 3) showed a strong gradient below 2000 m (a.s.l.). Because of
297  the valley geography, with surrounding mountains of about ~2000 m (a.s.l.) or higher, it is likely that the
298  gradient observed below 2000 m (a.s.l.) could be related to emissions from the Pokhara Valley. The
299  development (or dissolution) of the boundary layer during the day clearly influenced the evolution of
300  the aerosol vertical profiles in the Pokhara Valley. The shallow boundary layer in the night, which
301  continued till the morning, led to the accumulation of aerosols below 2000 m (a.s.l.) in the morning (see
302  the morning flights (F1, F3, and F5) and a strong decrease with altitude was observed. For instance, in
303  the morning profiles, the concentrations near the surface (<1000 m a.s.l.) for total particle number
304  concentrations (also indicated as **TPC** in Figure 4) were mostly >$10^3$ cm$^{-3}$, but could reach ~ 3x$10^4$ cm$^{-3}$ or
305  higher (see F5 in Figure 4), which is  attributed to the coupling of the shallow boundary layer and the
306  emissions in the contained valley topography (Mues et al., 2017). Also, all the measured aerosol
307  parameters (number size distribution for particles with diameters between 0.3 and 0.5 µm), the total
308  particle concentration (>14 nm), and the absorption) vary similarly as a function of the altitude
309  irrespective of the timing of the profiles. The similarity in the vertical concentration gradients of the
310  absorbing aerosol mass concentrations and the aerosol number concentration above 2000 m (a.s.l.)
311  provides evidence of similar emission sources or origins.

312      Within the morning profiles, substantial variations were observed; in F1 (5 May), in addition to the
313  strong gradient below 2000 m (a.s.l.), there is a polluted layer above 3000 m (a.s.l.) which is not evident
314  in F5. The BC concentration was close to 1 µgm$^{-3}$ up to 4000 m (a.s.l.) for F1 and stayed in that range
315  until F5, where it dropped to about ~0.4 µgm$^{-3}$. The temperature and humidity profile also showed
316  changes between the morning flights; the conditions during F1 are warmer (throughout the profile) and
317  dryer (near the surface), compared to F5.  This observed variation in the aerosol vertical profile
318  (including the meteorology) may be indicative of cleaner atmospheric conditions (in terms of aerosol
319  number and absorption) from 5 May to 7 May and could be associated with the arrival of colder
320  airmasses in the Pokhara Valley. The near-surface BC concentrations measured in this study were much
321  lower than surface BC concentrations measured in the pre-monsoon season (2013) in the Kathmandu
322  Valley in the Himalayan foothills (hourly average: ~5-40 µgm$^{-3}$, Mues et al. (2017)), but comparable to
323  winter measurements (2004) in Kanpur in the IGP (1-3 min average: ~1-7 µgm$^{-3}$, Tripathi et al. (2005)). In

324    Kanpur, Tripathi et al. (2005) observed BC concentrations close to 1 μgm$^{-3}$ up to 2000 m (a.s.l.) and a

325    sharp gradient below 400 m (a.s.l.), most likely due to a shallow boundary layer in winter.

326    The elevated polluted air mass in F1 could be an indication of transport related to the mountain

327    valley winds and/or synoptic transport related to the westerlies, common during this season (Gautam et

328    al., 2011;Raatikainen et al., 2014;Marcq et al., 2010). Pre-monsoon airborne measurements over the IGP

329    and near the Himalayan foothills during CALIPEX-2009 found a polluted aerosol layer (2-4x10$^{3}$ cm$^{-3}$ with

330    a mean size of 0.13 μm diameter) below 4 km (a.s.l), attributed to biomass burning observed during this

331    particular season (Padmakumari et al., 2013).

332    The afternoon profiles (F2: 5 May 2016 and F4: 6 May 2016)  in contrast to the corresponding

333    morning profile (F1 and F3) showed a more relatively mixed profile up to about 2500-3000 m, decreased

334    then up to the maximum sampled altitude of just above 4000 m (a.s.l.). For instance, the concentrations

335    of measured aerosol parameters up to 3000 m (a.s.l.) were comparable to the concentrations observed

336    at ~1000 m (a.s.l.). Slight differences exist within the afternoon profiles, which may be related to local

337    meteorology (boundary layer evolution) and mountain valley wind circulation in the afternoon. Cloud

338    layers were present during the afternoon flights at and above 4000 m (a.s.l.) in F4 (also indicated by the

339    sharp rise in RH from ca. 3600 m a.s.l.), which may have led to the scavenging of the aerosol by cloud

340    droplets and thus explaining the observed decrease in the measured aerosol parameters.

341    3.2.2.    Nature of absorbing aerosols in the Pokhara Valley

342    The absorption at multiple wavelengths was used to calculate the absorption Ångstrom exponent

343    (AAE), shown in the right-most subplot in each row of Figure 4. AAE characterizes the wavelength (λ)

344    dependence of absorption coefficient ($\text{Absorption coefficient or Abs. coeff} = \text{K}\lambda^{-\text{AAE}}$, Russell et al.

345    (2010);Giles et al. (2012)).  On a logarithmic scale, the above power relation between (Absorption

346    coefficient and wavelength) is approximately a straight line (see supplementary S11 for an example case

347    where both power and logarithmic form are plotted).  The slope of the straight line is AAE. In our case,

348    all the absorption coefficient measured between the 470 and 880 nm wavelength was used for the

349    calculation of AAE. The mass absorption coefficients (MAC) of 14.5 and 7.77 m$^{2}$g$^{-1}$, as prescribed by the

350    manufacturer of the aethalometer (Hansen et al., 1984) for wavelength 470 nm and 880 nm,

351    respectively were used to calculate the absorption coefficient (the unit for the absorption coefficient is

352    m$^{-1}$). The calculated AAE was averaged for each 100 m (a.s.l.), as shown in the figure. The sampling

353    resolution for the aethalometer is 2 min (see Table 1), which resulted in no (in a few cases) or few data

12

354   (after flagging) if smaller height bins were chosen. The AAE profile differed markedly between the

355   morning (F1, F3, and F5) and afternoon (F2 and F4) profiles, with morning profiles showed large

356   variations along the height. Surface AAE (~1000 m a.s.l.) was close to 0.8 to 1.2 for all the flights which

357   indicate the presence of BC from a mix of sources (biomass burning and fossil fuel combustion.  A

358   source-diagnostic analysis of C-isotopes of elemental carbon (EC) in TSP (total suspended particulates)

359   collected in Pokhara during April 2013-March 2014 showed that the biomass burning and fossil fuel

360   combustion contributes nearly 50 % each to the (annual average) EC concentration (Li et al., 2016). The

361   AAE values above surface (>1000 m a.s.l.) varied from 0.5 to 2,  but mostly fell into the range of 0.9- 1.2,

362   which is typically reported  for mixed to *BC like* aerosols from urban and industrial emissions (Russell et

363   al., 2010;Yang et al., 2009;Dumka et al., 2014). AAE<1 could also be indicative of a composite aerosol,

364   where a BC aerosol  (or "core") is coated with absorbing or non-absorbing aerosols (Gyawali et al.,

365   2009).

366   **Figure 5**. Aerosol extinction coefficient (at 532 nm) vertical profile (left) and aerosol type

367   classification based on the CALIPSO level 2 retrieval (right).  Only the CALIPSO overpass over the Pokhara

368   Valley or nearby locations (such as Kathmandu Valley region, and the region to the west of Pokhara

369   Valley) is included. The extinction profile is averaged for the region 27-28.5° N latitude, which also

370   includes the Pokhara Valley.

371   3.2.3.   Comparison of the satellite-derived vertical profiles with measurements

372   The measured vertical profiles were also complemented with CALIPSO retrievals over the Pokhara

373   Valley (Figure 5). Level 2 (version 4), cloud and quality screened data were used to generate the

374   vertically resolved extinction (at 532 nm) and aerosol classification. The CALIPSO satellite had only three

375   overpasses over the Pokhara Valley between 1 and 10 May 2016 (the extinction profile lines with circle

376   markers are for the Pokhara Valley). Therefore, the satellite overpasses through nearby regions such as

377   the Kathmandu Valley region to the east and the region to the west of the Pokhara Valley (denoted by

378   *WestPV* in Figure 5) were also considered.  The range of extinction values for the Pokhara Valley (0.15-

379   0.25 km$^{-1}$ especially around 2000-4000 m a.s.l.) were similar to pre-monsoon values (0.15-3 km$^{-1}$)

380   reported in Nainital (a hilly station located ~2000 m (a.s.l.) in India, and 400 km west of the Pokhara

381   Valley) and slightly less than Kanpur, a site in the IGP, about 400 km to the southwest of Pokhara

382   (Dumka et al., 2014). A large extinction (>0.5 km$^{-1}$ ) was observed on 1 May 2016 over the Pokhara

383   Valley at an altitude of 3-4 km (a.s.l.) which can be attributed to smoke (biomass- related) and polluted

384   dust (a mixture of dust and biomass smoke or urban pollution) as evident by the aerosol type

385    classification. Aerosols over the IGP and in the proximity of the Himalayan foothills were mainly "Dust"

386    on 1 May 2016. Although not conclusive, the 9 May aerosol type classification is markedly different from

387    1 May with the absence of dust in the IGP, and absence of polluted dust or smoke over the Pokhara

388    Valley.

389    **Figure 6**. HYSPLIT (Hybrid Single Particle Lagrangian Integrated Trajectory, Draxler and Hess (1998)) 3

390    day back trajectories of air masses arriving at 3 different heights (800 m, 1500 m and 2500 m) from

391    above the ground level (AGL~ 815 m a.s.l.) in the Pokhara Valley (28.19° N, 83.98° E) during 5-7 May

392    2016. NCEP GDAS (Global Data Assimilation System) Reanalysis data with 1°x1° horizontal resolution

393    were used as the input meteorology. The trajectory data is overlayed with the active fire data

394    (extracted from the MODIS collection 6 database, available at

395    https://firms2.modaps.eosdis.nasa.gov/active_fire. Each green dot with a gray edge is an active fire, and

396    the strength of the active fire is indicated by the "*frp" value,* which is the fire radiative power in

397    megawatts.

398    3.2.4.   Role of synoptic circulation in modulating aerosol properties over the Pokhara Valley

399    The measured vertical profiles and available satellite data from MODIS (See Figure S8) and CALIPSO

400    suggest that the synoptic-scale circulation were changing during the study period. The changing synoptic

401    circulation also influenced the transport of polluted air into the Pokhara Valley. The regional

402    meteorology station in the Pokhara Valley reported hazy conditions till 5 May 2016(see Figure S6) which

403    disappeared from 6 May 2016 onwards followed by clear days with scattered clouds during the daytime

404    and thunderstorms in the afternoon. The variation in the AOD, AOD-F and Fine Mode Fraction (FMF)

405    from AERONET (only level 1.5 data were available, see Figure S7) also showed that high turbidity in the

406    atmospheric column, dominated by fine-mode aerosols before 5 May 2016 ($AOD_{500nm}$>2.0, FMF >0.9),

407    which declined sharply after 5 May 2016. The variation in the horizontal visibility (or visual range)

408    measured at the meteorology station in the Pokhara Valley further indicates that the intensity of

409    pollution declined during the study period, especially starting on 5 May 2016.

410    Three day back trajectories (72 h) were generated using HYSPLIT (Hybrid Single Particle Lagrangian

411    Integrated Trajectory) for air masses arriving in the Pokhara Valley at 800 m, 1,500 m and 2,500 m from

412    above ground level (AGL) for the test flight period (see Figure 6). The NCEP GDAS reanalysis data with a

413    1°x1° horizontal resolution were used as the input meteorology for the trajectories. The majority of air

414    masses (especially at 1500 and 2000 m AGL) were westerly. A high resolution (0.0625° horizontal)

415    simulation of air mass trajectories during the pre-monsoon period over the Himalayas and Tibetan

416    Plateau region by Lüthi et al. (2015) also identified synoptic-scale transport (as westerly advection

417    around 500 mb) and a convection-enabled polluted airmass  from the IGP as a major mechanism of

418    transport of air pollution in the Himalayas. Transport of air pollution by both mechanisms was coupled

419    with the diurnal expansion of PBL height in the IGP where the trajectory height was similar to planetary

420    boundary layer (PBL) height thus allowing mixing up of the polluted layer, also observed by Raatikainen

421    et al. (2014) over Gual Pahari (IGP site) and Mukteswor (Himalayan foothill site).

422        During the study period, the direction of the trajectories varied as the air masses entered Nepal and

423    eventually into the Pokhara Valley. On 5 and 6 May 2016, the air masses (at 1500 and 2000 m AGL) were

424    mostly northwesterly traversing through northern India and western Nepal before entering the Pokhara

425    Valley. A shift in the trajectory direction from north westerly to south westerly was observed on 7 May

426    2016, where the trajectories were moving through central India and the southern foothills into the

427    Pokhara Valley. The observed shift in the trajectories at 1500 and 2500 m AGL was modulated by the

428    synoptic-scale changes in the mid-latitude (over Central Asia) air masses (40-50° N) (Lüthi et al., 2015).

429    The intrusion (in the form of a trough) of the cold and humid air masses from 40-50° N (see Figure 2)

430    into 20-30° N occurred during the study period. As the trough moves eastward, it shifts the synoptic air

431    mass at 20-30° N from northwesterly to southwesterly on 7 May 2016. The elevated polluted layer on 5

432    and 6 May 2016 (Figure 4) could be the result of this modulation of the westerly. The northwesterly

433    airmass entered Nepal via Northern India, where MODIS retrievals showed a high aerosol loading (See

434    Figure S8), which could be mainly attributed to the numerous biomass fire events (See Figure S9)

435    observed in North India.  In addition, numerous forest fires were also reported in western Nepal during

436    the same period. However, the absorption signal from the flight measurement does not clearly show

437    higher absorption at shorter wavelengths compared to absorption at 880 or longer wavelengths. This

438    also implies that the observed elevated polluted layer in the Pokhara Valley is not entirely due to the

439    biomass burning plume intercepted by the westerlies or north-westerlies. As the airmass origin shifts to

440    southwesterly on 7 May 2016 (detected during flight F5), the synoptic air mass bypassed the high AOD

441    loading over north India and contained the cold and relatively clean air from Central Asia. This resulted

442    in the disappearance of the polluted layer over 2000 m (a.s.l.) during flight F5.

443    *4.*    **Conclusion**

444        This paper provides an overview of the pre-monsoon airborne measurement carried out with a

445    microlight aircraft platform in the Pokhara Valley in Nepal, the first-of-their-kind airborne aerosol

446   measurements in the Himalayan foothill region. The objective of the overall airborne campaign in the

447   Himalayan region was to quantify the vertical distribution of aerosols over a polluted mountain valley

448   region, as well as to measure the extent of regional transport into the Himalayas. In this paper,

449   measurements from the test flights during May 2016 are summarized. These mainly include vertical

450   profiles of aerosol number and size distribution, multi-wavelength aerosol absorption, black carbon,

451   total particle concentration, and meteorological variables. The instrument package, designed for a

452   microlight sampling was fitted to an IKARUS-C42 microlight aircraft. A total of five test flights were

453   conducted between 5 and 7 May 2016, including morning and evening flights for about 1-1.5 h each, as

454   well as vertical spirals to characterize vertical profiles of aerosols and meteorological parameters

455        The results presented in this paper should be considered as a pilot study mapping out the

456   aerosol concentrations and their interactions with meteorological processes in the Pokhara Valley due

457   to the limited flight time.  In all the measured flights, the vertical profiles of aerosol parameters showed

458   strong gradients along the atmospheric column. The observed total number concentration gradient was

459   strongly influenced by the mountain valley boundary layer, which resulted in a sharp gradient below

460   about 1500-2000 m (a.s.l.). The increase of boundary layer height contributed to the differences in the

461   morning and afternoon profiles.  Similar vertical profiles of BC concentrations and aerosol total particle

462   number concentrations provided evidence of common emission sources or co-located origins. The

463   observed BC concentration near the surface (~ 1000 m a.s.l.) was much lower than pre-monsoon BC

464   concentrations measured in the Kathmandu Valley but comparable to values reported during the winter

465   season in Kanpur in the IGP.  The AAE estimates near the surface, based on the absorption value, fell in

466   the range of 0.9-1.2, which indicates the presence of *BC like* and mixed (dust, urban, biomass) aerosols.

467   An elevated polluted layer was observed at around 3 km (a.s.l.) over the Pokhara Valley during this

468   study. Characterized by a strong presence of dust in the IGP and polluted continental airmasses over the

469   Pokhara Valley, the polluted layer could be linked with the westerly synoptic circulations and regional

470   transport from the IGP and surrounding regions. The direction of the synoptic transport entering the

471   Himalayan foothills and into Pokhara Valley, however, was influenced by the Westerlies at mid-latitudes

472   (40-50° N). The extent of transport can be better quantified with regional airborne measurements along

473   the south-north transect through the region between the IGP and the Himalayan foothills at high

474   altitudes in the Himalayas, including the Pokhara Valley.  We will explore the extent of such regional

475   transport in a subsequent publication that will be primarily based on the airborne measurements in

476   phase II (December 2016- January 2017) in the Pokhara Valley and in the surrounding region. The

477 subsequent paper will also characterize the extent of vertical transport from three different mountain

478 valleys located at different elevations along the south-north transect.

## *5.* References

489 Aryal, D., Rosoff, Y. N., and Devkota, L. P.: A Severe Hailstorm at Pokhara: CAPE Stability Index
490 Calculations, Journal of Geosciences and Geomatics, 3, 142-153, 2015.
491 Bollasina, M. A., Ming, Y., and Ramaswamy, V.: Anthropogenic Aerosols and the Weakening of the South
492 Asian Summer Monsoon, Science, 334, 502-505, 10.1126/science.1204994, 2011.
493 Brauer, M., Amann, M., Burnett, R. T., Cohen, A., Dentener, F., Ezzati, M., Henderson, S. B.,
494 Krzyzanowski, M., Martin, R. V., Van Dingenen, R., van Donkelaar, A., and Thurston, G. D.: Exposure
495 assessment for estimation of the global burden of disease attributable to outdoor air pollution,
496 Environmental science & technology, 46, 652-660, 10.1021/es2025752, 2012.
497 Burney, J., and Ramanathan, V.: Recent climate and air pollution impacts on Indian agriculture,
498 Proceedings of the National Academy of Sciences, 111, 16319-16324, 10.1073/pnas.1317275111, 2014.
499 Cho, C., Kim, S. W., Rupakheti, M., Park, J. S., Panday, A., Yoon, S. C., Kim, J. H., Kim, H., Jeon, H., Sung,
500 M., Kim, B. M., Hong, S. K., Park, R. J., Rupakheti, D., Mahata, K. S., Praveen, P. S., Lawrence, M. G., and
501 Holben, B.: Wintertime aerosol optical and radiative properties in the Kathmandu Valley during the
502 SusKat-ABC field campaign, Atmos. Chem. Phys., 17, 12617-12632, 10.5194/acp-17-12617-2017, 2017.
503 Cong, Z., Kawamura, K., Kang, S., and Fu, P.: Penetration of biomass-burning emissions from South Asia
504 through the Himalayas: new insights from atmospheric organic acids, 5, 9580, 10.1038/srep09580

505 http://dharmasastra.live.cf.private.springer.com/articles/srep09580#supplementary-information, 2015.
506 Decesari, S., Facchini, M. C., Carbone, C., Giulianelli, L., Rinaldi, M., Finessi, E., Fuzzi, S., Marinoni, A.,
507 Cristofanelli, P., Duchi, R., Bonasoni, P., Vuillermoz, E., Cozic, J., Jaffrezo, J. L., and Laj, P.: Chemical
508 composition of PM$_{10}$ and PM$_1$ at the high-altitude Himalayan station Nepal
509 Climate Observatory-Pyramid (NCO-P) (5079 m a.s.l.), Atmos. Chem. Phys., 10, 4583-4596, 10.5194/acp-
510 10-4583-2010, 2010.
511 Dey, S., and Di Girolamo, L.: A climatology of aerosol optical and microphysical properties over the
512 Indian subcontinent from 9 years (2000–2008) of Multiangle Imaging Spectroradiometer (MISR) data,
513 Journal of Geophysical Research: Atmospheres, 115, n/a-n/a, 10.1029/2009JD013395, 2010.
514 Draxler, R. R., and Hess, G. D.: An overview of the HYSPLIT_4 modeling system for trajectories,
515 dispersion, and deposition, Aust. Meteor. Mag, 47, 295–230, 1998.

516    Dumka, U. C., N. Tripathi, S., Misra, A., Giles, D. M., Eck, T. F., Sagar, R., and Holben, B. N.: Latitudinal
517    variation of aerosol properties from Indo-Gangetic Plain to central Himalayan foothills during TIGERZ
518    campaign, Journal of Geophysical Research: Atmospheres, 119, 4750-4769, 10.1002/2013jd021040,
519    2014.
520    Gautam, R., Hsu, N. C., Lau, K. M., and Kafatos, M.: Aerosol and rainfall variability over the Indian
521    monsoon region: distributions, trends and coupling, Ann. Geophys., 27, 3691-3703, 10.5194/angeo-27-
522    3691-2009, 2009a.
523    Gautam, R., Hsu, N. C., Lau, K. M., Tsay, S. C., and Kafatos, M.: Enhanced pre-monsoon warming over the
524    Himalayan-Gangetic region from 1979 to 2007, Geophysical Research Letters, 36, n/a-n/a,
525    10.1029/2009GL037641, 2009b.
526    Gautam, R., Hsu, N. C., Tsay, S. C., Lau, K. M., Holben, B., Bell, S., Smirnov, A., Li, C., Hansell, R., Ji, Q.,
527    Payra, S., Aryal, D., Kayastha, R., and Kim, K. M.: Accumulation of aerosols over the Indo-Gangetic plains
528    and southern slopes of the Himalayas: distribution, properties and radiative effects during the 2009 pre-
529    monsoon season, Atmospheric Chemistry and Physics, 11, 12841-12863, 10.5194/acp-11-12841-2011,
530    2011.
531    Giles, D. M., Holben, B. N., Eck, T. F., Sinyuk, A., Smirnov, A., Slutsker, I., Dickerson, R. R., Thompson, A.
532    M., and Schafer, J. S.: An analysis of AERONET aerosol absorption properties and classifications
533    representative of aerosol source regions, Journal of Geophysical Research: Atmospheres, 117, n/a-n/a,
534    10.1029/2012jd018127, 2012.
535    Gogoi, M. M., Moorthy, K. K., Kompalli, S. K., Chaubey, J. P., Babu, S. S., Manoj, M. R., Nair, V. S., and
536    Prabhu, T. P.: Physical and optical properties of aerosols in a free tropospheric environment: Results
537    from long-term observations over western trans-Himalayas, Atmospheric Environment, 84, 262-274,
538    https://doi.org/10.1016/j.atmosenv.2013.11.029, 2014.
539    Guttikunda, S. K., Goel, R., and Pant, P.: Nature of air pollution, emission sources, and management in
540    the Indian cities, Atmospheric Environment, 95, 501-510,
541    http://dx.doi.org/10.1016/j.atmosenv.2014.07.006, 2014.
542    Gyawali, M., Arnott, W. P., Lewis, K., and Moosmüller, H.: In situ aerosol optics in Reno, NV, USA during
543    and after the summer 2008 California wildfires and the influence of absorbing and non-absorbing
544    organic coatings on spectral light absorption, Atmos. Chem. Phys., 9, 8007-8015, 10.5194/acp-9-8007-
545    2009, 2009.
546    Hansen, A. D. A., Rosen, H., and Novakov, T.: The aethalometer — An instrument for the real-time
547    measurement of optical absorption by aerosol particles, Science of The Total Environment, 36, 191-196,
548    https://doi.org/10.1016/0048-9697(84)90265-1, 1984.
549    Jai Devi, J., Tripathi, S. N., Gupta, T., Singh, B. N., Gopalakrishnan, V., and Dey, S.: Observation-based 3-D
550    view of aerosol radiative properties over Indian Continental Tropical Convergence Zone: implications to
551    regional climate, Tellus B, 63, 971-989, 10.1111/j.1600-0889.2011.00580.x, 2011.
552    Junkermann, W.: An Ultralight Aircraft as Platform for Research in the Lower Troposphere: System
553    Performance and First Results from Radiation Transfer Studies in Stratiform Aerosol Layers and Broken
554    Cloud Conditions, Journal of Atmospheric and Oceanic Technology, 18, 934-946, 10.1175/1520-
555    0426(2001)018<0934:auaapf>2.0.co;2, 2001.
556    Kaskaoutis, D. G., Singh, R. P., Gautam, R., Sharma, M., Kosmopoulos, P. G., and Tripathi, S. N.: Variability
557    and trends of aerosol properties over Kanpur, northern India using AERONET data (2001–10),
558    Environmental Research Letters, 7, 024003, 10.1088/1748-9326/7/2/024003, 2012.
559    Kuhlmann, J., and Quaas, J.: How can aerosols affect the Asian summer monsoon? Assessment during
560    three consecutive pre-monsoon seasons from CALIPSO satellite data, Atmos. Chem. Phys., 10, 4673-
561    4688, 10.5194/acp-10-4673-2010, 2010.
562    Lau, W.: Atmospheric science: Desert dust and monsoon rain, Nature Geosci, 7, 255-256,
563    10.1038/ngeo2115, 2014.

Lawrence, M. G., and Lelieveld, J.: Atmospheric pollutant outflow from southern Asia: a review, Atmos. Chem. Phys., 10, 11017-11096, 10.5194/acp-10-11017-2010, 2010.

Li, C., Bosch, C., Kang, S., Andersson, A., Chen, P., Zhang, Q., Cong, Z., Chen, B., Qin, D., and Gustafsson, O.: Sources of black carbon to the Himalayan-Tibetan Plateau glaciers, Nat Commun, 7, 12574, 10.1038/ncomms12574, 2016.

Lüthi, Z. L., Škerlak, B., Kim, S. W., Lauer, A., Mues, A., Rupakheti, M., and Kang, S.: Atmospheric brown clouds reach the Tibetan Plateau by crossing the Himalayas, Atmos. Chem. Phys., 15, 6007-6021, 10.5194/acp-15-6007-2015, 2015.

Marcq, S., Laj, P., Roger, J. C., Villani, P., Sellegri, K., Bonasoni, P., Marinoni, A., Cristofanelli, P., Verza, G. P., and Bergin, M.: Aerosol optical properties and radiative forcing in the high Himalaya based on measurements at the Nepal Climate Observatory-Pyramid site (5079 m a.s.l.), Atmos. Chem. Phys., 10, 5859-5872, 10.5194/acp-10-5859-2010, 2010.

Marinoni, A., Cristofanelli, P., Laj, P., Duchi, R., Putero, D., Calzolari, F., Landi, T. C., Vuillermoz, E., Maione, M., and Bonasoni, P.: High black carbon and ozone concentrations during pollution transport in the Himalayas: Five years of continuous observations at NCO-P global GAW station, Journal of Environmental Sciences, 25, 1618-1625, http://dx.doi.org/10.1016/S1001-0742(12)60242-3, 2013.

Mues, A., Rupakheti, M., Münkel, C., Lauer, A., Bozem, H., Hoor, P., Butler, T., and Lawrence, M. G.: Investigation of the mixing layer height derived from ceilometer measurements in the Kathmandu Valley and implications for local air quality, Atmos. Chem. Phys., 17, 8157-8176, 10.5194/acp-17-8157-2017, 2017.

Neitola, K., Asmi, E., Komppula, M., Hyvärinen, A. P., Raatikainen, T., Panwar, T. S., Sharma, V. P., and Lihavainen, H.: New particle formation infrequently observed in Himalayan foothills – why?, Atmos. Chem. Phys., 11, 8447-8458, 10.5194/acp-11-8447-2011, 2011.

Padmakumari, B., Maheskumar, R. S., Morwal, S. B., Harikishan, G., Konwar, M., Kulkarni, J. R., and Goswami, B. N.: Aircraft observations of elevated pollution layers near the foothills of the Himalayas during CAIPEEX-2009, Quarterly Journal of the Royal Meteorological Society, 139, 625-638, 10.1002/qj.1989, 2013.

Panday, A. K., and Prinn, R. G.: Diurnal cycle of air pollution in the Kathmandu Valley, Nepal: Observations, Journal of Geophysical Research: Atmospheres, 114, D09305, 10.1029/2008JD009777, 2009.

Pandey, S. K., Vinoj, V., Landu, K., and Babu, S. S.: Declining pre-monsoon dust loading over South Asia: Signature of a changing regional climate, Scientific Reports, 7, 16062, 10.1038/s41598-017-16338-w, 2017.

Putero, D., Landi, T. C., Cristofanelli, P., Marinoni, A., Laj, P., Duchi, R., Calzolari, F., Verza, G. P., and Bonasoni, P.: Influence of open vegetation fires on black carbon and ozone variability in the southern Himalayas (NCO-P, 5079 m a.s.l.), Environ Pollut, 184, 597-604, 10.1016/j.envpol.2013.09.035, 2014.

Putero, D., Cristofanelli, P., Marinoni, A., Adhikary, B., Duchi, R., Shrestha, S. D., Verza, G. P., Landi, T. C., Calzolari, F., Busetto, M., Agrillo, G., Biancofiore, F., Di Carlo, P., Panday, A. K., Rupakheti, M., and Bonasoni, P.: Seasonal variation of ozone and black carbon observed at Paknajol, an urban site in the Kathmandu Valley, Nepal, Atmos. Chem. Phys., 15, 13957-13971, 10.5194/acp-15-13957-2015, 2015.

Raatikainen, T., Hyvärinen, A. P., Hatakka, J., Panwar, T. S., Hooda, R. K., Sharma, V. P., and Lihavainen, H.: The effect of boundary layer dynamics on aerosol properties at the Indo-Gangetic plains and at the foothills of the Himalayas, Atmospheric Environment, 89, 548-555, 10.1016/j.atmosenv.2014.02.058, 2014.

Ramana, M. V., Ramanathan, V., Podgorny, I. A., Pradhan, B. B., and Shrestha, B.: The direct observations of large aerosol radiative forcing in the Himalayan region, Geophysical Research Letters, 31, n/a-n/a, 10.1029/2003GL018824, 2004.

611    Ramanathan, V., Crutzen, P. J., Kiehl, J. T., and Rosenfeld, D.: Aerosols, Climate, and the Hydrological
612    Cycle, Science, 294, 2119-2124, 10.1126/science.1064034, 2001.
613    Russell, P. B., Bergstrom, R. W., Shinozuka, Y., Clarke, A. D., DeCarlo, P. F., Jimenez, J. L., Livingston, J. M.,
614    Redemann, J., Dubovik, O., and Strawa, A.: Absorption Angstrom Exponent in AERONET and related data
615    as an indicator of aerosol composition, Atmos. Chem. Phys., 10, 1155-1169, 10.5194/acp-10-1155-2010,
616    2010.
617    Shrestha, P., Barros, A. P., and Khlystov, A.: Chemical composition and aerosol size distribution of the
618    middle mountain range in the Nepal Himalayas during the 2009 pre-monsoon season, Atmospheric
619    Chemistry and Physics, 10, 11605-11621, 2010.
620    Shrestha, P., Barros, A. P., and Khlystov, A.: CCN estimates from bulk hygroscopic growth factors of
621    ambient aerosols during the pre-monsoon season over Central Nepal, Atmospheric Environment, 67,
622    120-129, http://dx.doi.org/10.1016/j.atmosenv.2012.10.042, 2013.
623    Stone, E. A., Schauer, J. J., Pradhan, B. B., Dangol, P. M., Habib, G., Venkataraman, C., and Ramanathan,
624    V.: Characterization of emissions from South Asian biofuels and application to source apportionment of
625    carbonaceous aerosol in the Himalayas, Journal of Geophysical Research: Atmospheres, 115, n/a-n/a,
626    10.1029/2009JD011881, 2010.
627    Tripathi, S. N., Dey, S., Tare, V., Satheesh, S. K., Lal, S., and Venkataramani, S.: Enhanced layer of black
628    carbon in a north Indian industrial city, Geophysical Research Letters, 32, n/a-n/a,
629    10.1029/2005gl022564, 2005.
630    Venkataraman, C., Habib, G., Kadamba, D., Shrivastava, M., Leon, J. F., Crouzille, B., Boucher, O., and
631    Streets, D. G.: Emissions from open biomass burning in India: Integrating the inventory approach with
632    high-resolution Moderate Resolution Imaging Spectroradiometer (MODIS) active-fire and land cover
633    data, Global Biogeochemical Cycles, 20, n/a-n/a, 10.1029/2005GB002547, 2006.
634    Venzac, H., Sellegri, K., Laj, P., Villani, P., Bonasoni, P., Marinoni, A., Cristofanelli, P., Calzolari, F., Fuzzi,
635    S., Decesari, S., Facchini, M. C., Vuillermoz, E., and Verza, G. P.: High frequency new particle formation in
636    the Himalayas, Proc Natl Acad Sci U S A, 105, 15666-15671, 10.1073/pnas.0801355105, 2008.
637    Vinoj, V., Rasch, P. J., Wang, H., Yoon, J.-H., Ma, P.-L., Landu, K., and Singh, B.: Short-term modulation of
638    Indian summer monsoon rainfall by West Asian dust, Nature Geosci, 7, 308-313, 10.1038/ngeo2107

639    http://www.nature.com/ngeo/journal/v7/n4/abs/ngeo2107.html#supplementary-information, 2014.
640    Xie, A., Ren, J., Qin, X., and Kang, S.: Reliability of NCEP/NCAR reanalysis data in the Himalayas/Tibetan
641    Plateau, Journal of Geographical Sciences, 17, 421-430, 10.1007/s11442-007-0421-2, 2007.
642    Yang, M., Howell, S. G., Zhuang, J., and Huebert, B. J.: Attribution of aerosol light absorption to black
643    carbon, brown carbon, and dust in China – interpretations of atmospheric measurements during EAST-
644    AIRE, Atmos. Chem. Phys., 9, 2035-2050, 10.5194/acp-9-2035-2009, 2009.

645

646

647 **List of Tables**

648 Table 1. Instrument package deployed in the microlight aircraft

| Parameters | Instruments | Method | Sampling time resolution |
|---|---|---|---|
| 1. Aerosol particle number size distribution (0.3 - 20 µm) | GRIMM 1.108 | Light scattering | 6 s |
| **2.** Total particle number concentration (>14 nm) | TSI CPC 3760 | Condensation/light scattering | 1 s |
| 3. Aerosol spectral absorption | Magee AE42 | 7 wavelengths, light attenuation | 2 min |
| 4. Dew point sensor | METEOLABOR, TPS3 | Chilled Mirror | 1 Hz |
| 5. Temperature | Thermocouple | - | 1 Hz |
| 6. Data acquisition system | PC 104+ GPS | --- | --- |
| 7. Power supply | Aircraft battery pack, LiFEPO$_4$ battery | 12 V, >15 AH | |

649
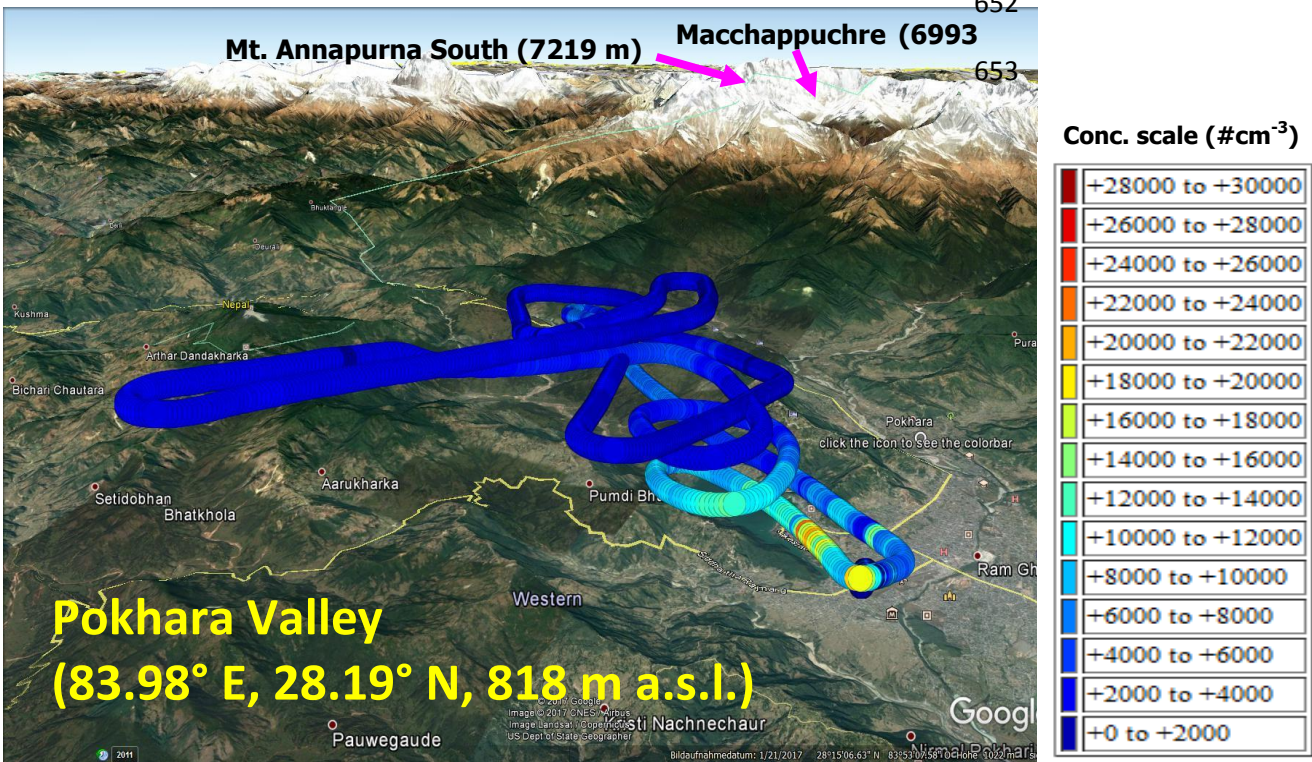
651



Figure 1. A typical test flight within the Pokhara Valley on 5 May 2016. The plot is generated using a Matlab-Google Earth toolbox (https://www.mathworks.com/matlabcentral/fileexchange/12954-google-earth-toolbox). Each dot is a single sample point (sampling frequency of 1Hz) and the color of the dot indicates the total aerosol number concentration (in # cm$^{-3}$) and the value of each color is shown as a color bar.
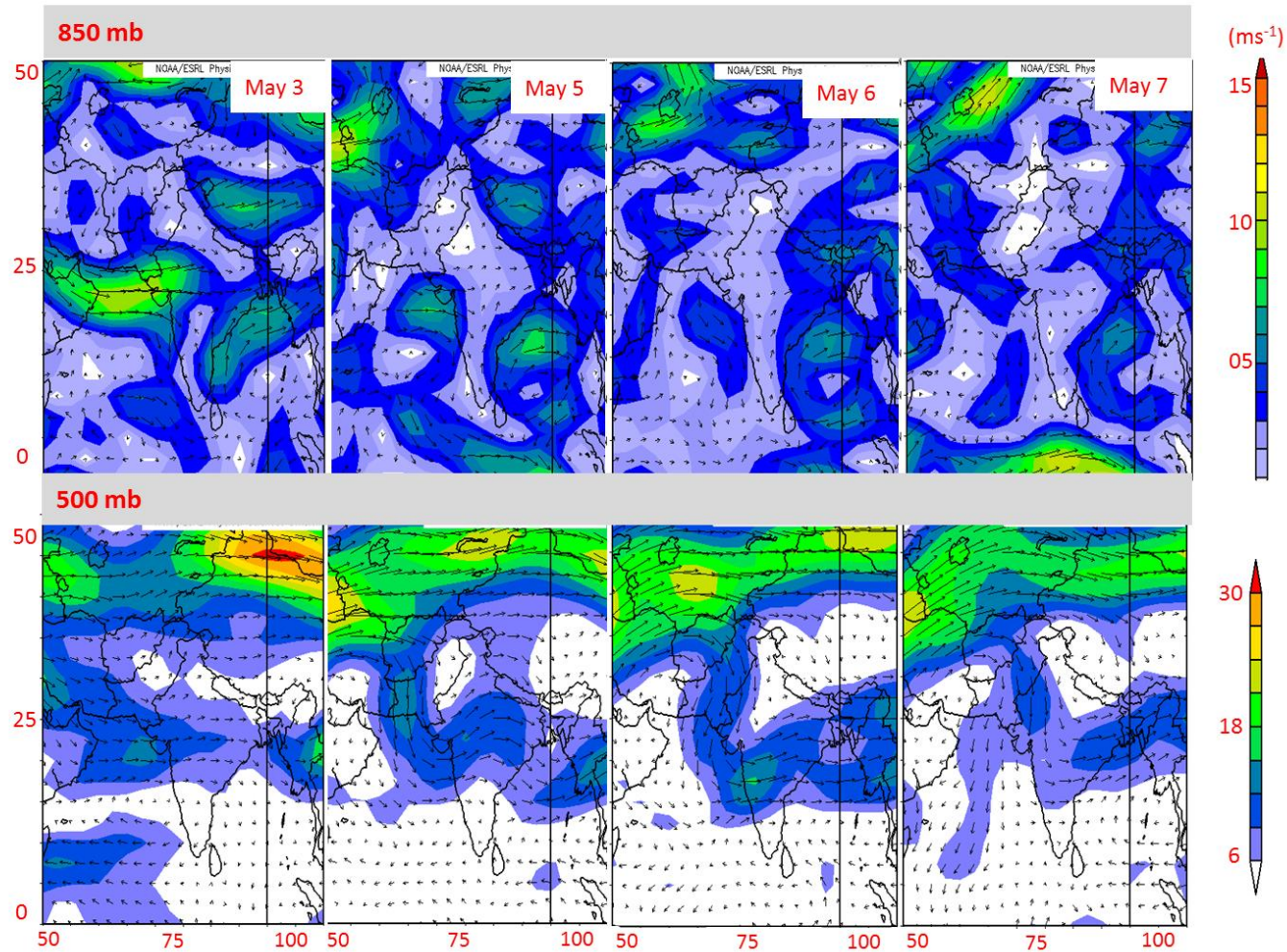
660

**Figure 2.** Daily wind vector data at 850 and 500 mb plotted using the NCEP NCAR reanalysis (2.5° x 2.5°) data over South Asia from 1-7 May

2016. The colors indicate the wind speed in ms^{-1}. The plots were generated using the default set-up at
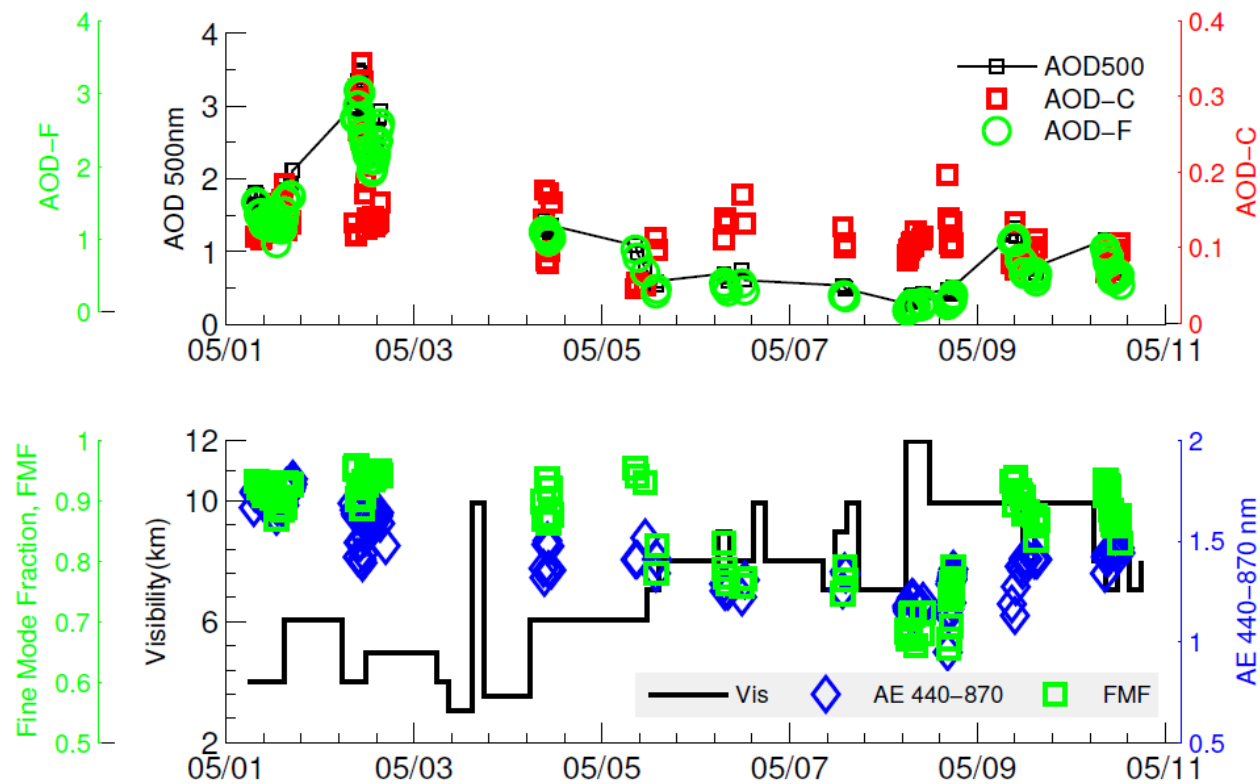
www.esrl.noaa.gov/psd/data/composites/day/.

664

665

**Figure 3.** AOD and other data products from the Level1.5 AERONET direct product in the Pokhara Valley from 1-10 May 2016. The top panel

includes AOD at 500nm and AOD coarse and fine (as shown in figure above as AOD-C, AOD-F). The bottom panel includes ångström Exponent

(AE) 440-870nm, fine mode fraction and visibility (km). The visibility data was available from the synoptic meteorology data available at the

http://www7.ncdc.noaa.gov/CDO/cdo

670

671    **Figure 4**

672

673



687

26
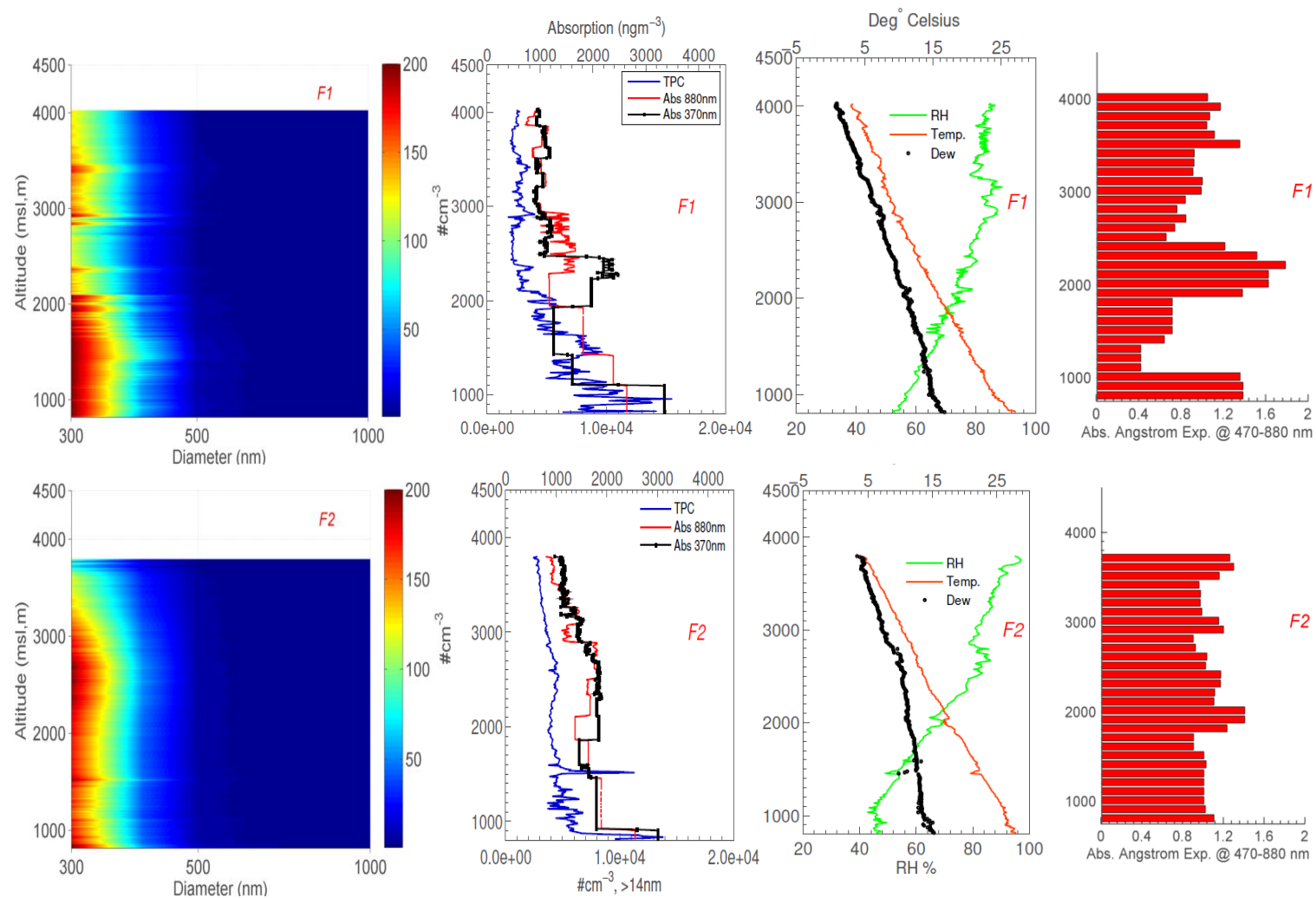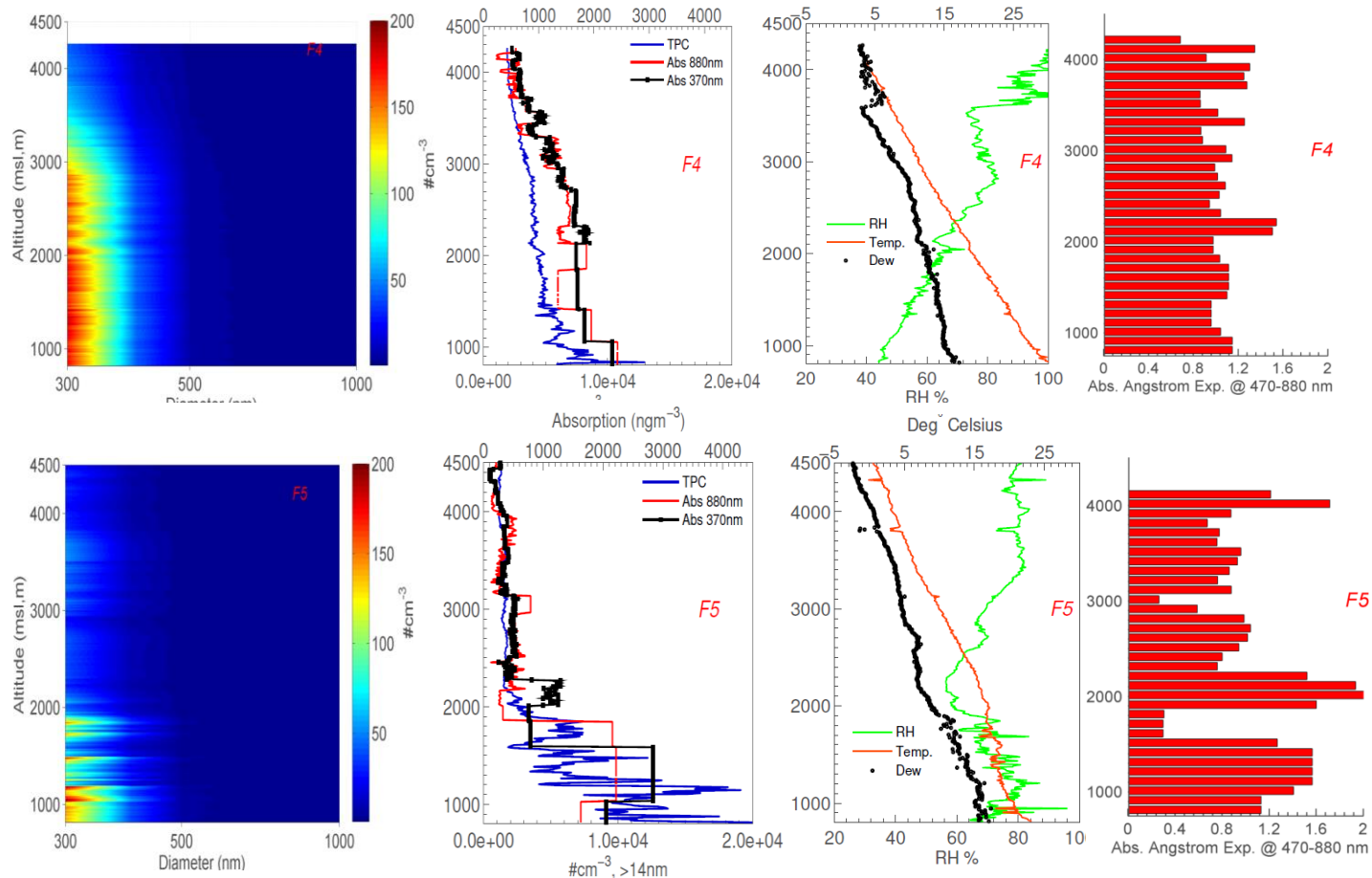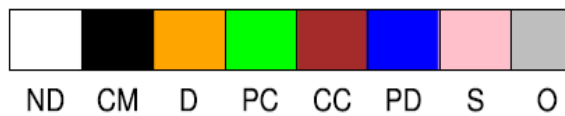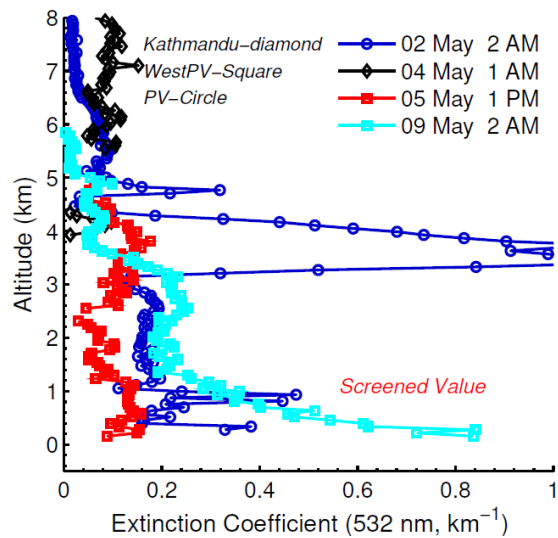
**Figure 4.** Vertical profiles of aerosol parameters and meteorological parameters during the 5-7 May 2016 test flights in the Pokhara Valley using the IKARUS microlight aircraft. The subplot in each row is arranged by (**i**) Aerosol number size distribution measured by the Grimm OPC 1.108 (0.3-20 µm), limited to 1 µm in the figure, (**ii**) Total particle number concentration (also indicated as *TPC*, Dp >14 nm) measured by the CPC 3760 and absorption aerosol at 370 nm and 880 nm (**iii**) temperature (°C) and dew point (black dot, in °C) and relative humidity (or RH %), (**iv**) calculated absorption Ångstrom exponent averaged for every 500 meters elevation band. For the size distribution plot, the x-axis represents the

693     optical diameter of the aerosol (nm), and the color bar represents the concentration ($10^x$ in #cm$^{-3}$). Of the five test flights, only F1-2, F4-5 is

694     shown here, F3 is in the supplementary. Number size distribution data from Flight F3 is not available due to the failure of the Grimm's pump

695     during flight initiation. In each subplot, the y-axis is the altitude above the mean sea level (in m).  The origin of the y-axis is at 815 m (a.s.l.).

696

697

698

Pokhara Valley

*Kathmandu–diamond*
*WestPV–Square*
*PV–Circle*

| | |
|---|---|
| 02 May 2 AM | |
| 04 May 1 AM | |
| 05 May 1 PM | |
| 09 May 2 AM | |

*Screened Value*

Extinction Coefficient (532 nm, km$^{-1}$)

Pokhara Valley, 2 May

Kathmandu Valley, 4 May

West Pokhara Valley, 5 May

Pokhara Valley, 9 May

| ND | CM | D | PC | CC | PD | S | O |

**ND**-not detected, **CM**: clean Marine, **D**:dust
**PC:** Polluted Continental, **PD:** Polluted Dust;
**CC**: clean continental, **S**: Smoke, **O**:Others

699

29
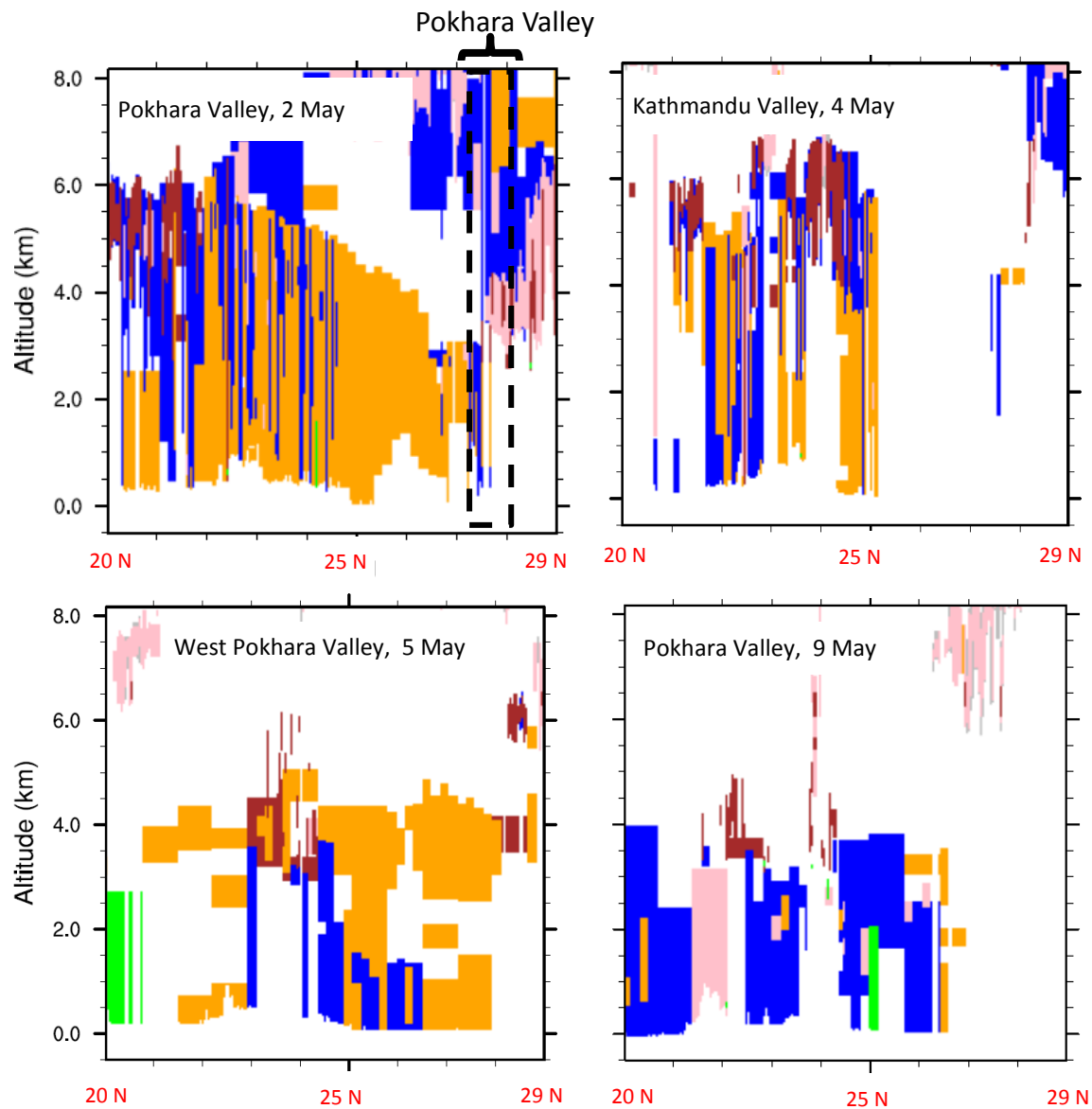
700 **Figure 5**. Aerosol extinction coefficient (at 532 nm) vertical profile (left) and aerosol type classification based on the CALIPSO level 2 retrieval

701 (right) available during May 2016.  Only the CALIPSO overpass over the Pokhara Valley or nearby locations (such as Kathmandu Valley region,

702 and the region to west of Pokhara Valley) are included). The extinction profile is averaged for the region 27-28.5° N latitude which also includes
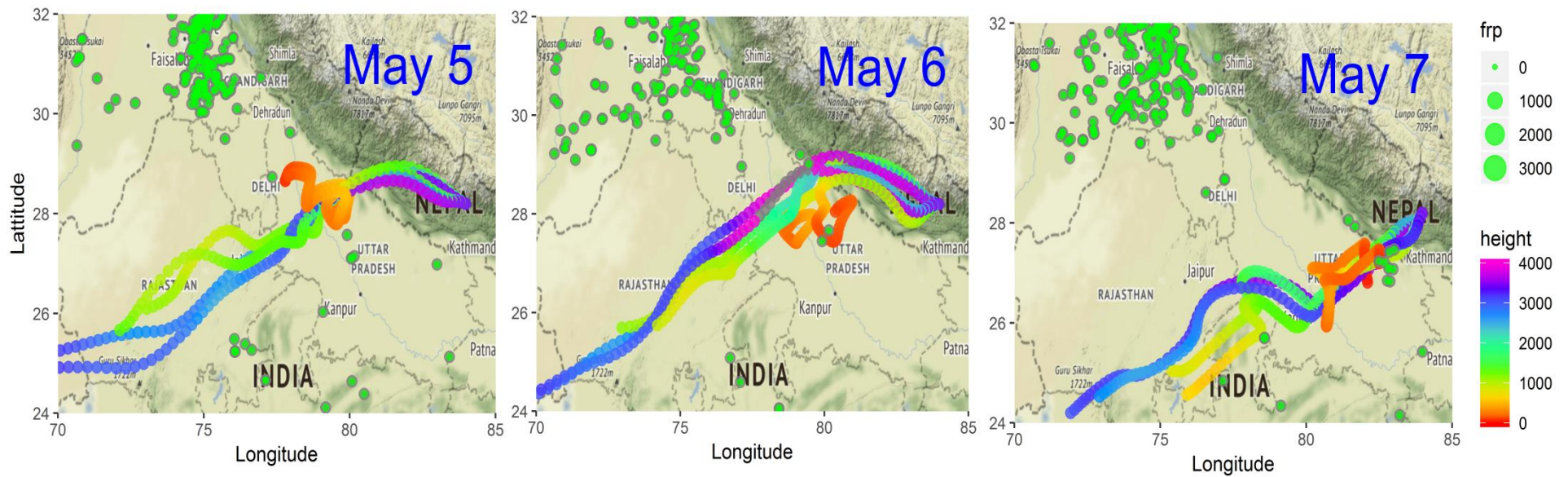
703 the Pokhara Valley.

704

**Figure 6**. HYSPLIT (Hybrid Single Particle Lagrangian Integrated Trajectory) 3 day back trajectories of air masses arriving at 3 different heights (800 m, 1500 m and 2500 m) from above the ground level (AGL~ 815 m a.s.l.) in the Pokhara Valley (28.19° N, 83.98° E) during 5-7 May 2016. NCEP GDAS (Global Data Assimilation System) Reanalysis data with 1°x1° horizontal resolution were used as the input meteorology. The trajectory data is overlayed with the active fire data (extracted from the MODIS collection 6 database, available at https://firms2.modaps.eosdis.nasa.gov/active_fire . Each green dot with a gray edge is an active fire, and the strength of the active fire is indicated by the "*frp" value,* which is the fire radiative power in megawatts.